Vol 18 No 11, November 2009
1674-1056/2009/18(11)/4667-09

Chinese Physics B

© 2009 Chin. Phys. Soc.
and IOP Publishing Ltd

Strain distributions and electronic structure of three-dimensional InAs/GaAs quantum rings*

Liu Yu-Min(刘玉敏)†, Yu Zhong-Yuan(俞重远), Jia Bo-Yong(贾博雍),
Xu Zi-Huan(徐子欢), Yao Wen-Jie(姚文杰), Chen Zhi-Hui(陈智辉),
Lu Peng-Fei(芦鹏飞), and Han Li-Hong(韩利红)

Institute of Optical Communication and Optoelectronics, Beijing 100876, *China*
Key Laboratory of Information Photonics and Optical Communications (Beijing University of Posts and Telecommunications), Ministry of Education, Beijing 100876, *China*

(Received 31 July 2008; revised manuscript received 13 April 2009)

This paper presents a finite element calculation for the electronic structure and strain distribution of self-organized InAs/GaAs quantum rings. The strain distribution calculations are based on the continuum elastic theory. An ideal three-dimensional circular quantum ring model is adopted in this work. The electron and heavy-hole energy levels of the InAs/GaAs quantum rings are calculated by solving the three-dimensional effective mass Schrödinger equation including the deformation potential and piezoelectric potential up to the second order induced by the strain. The calculated results show the importance of strain and piezoelectric effects, and these effects should be taken into consideration in analysis of the optoelectronic characteristics of strain quantum rings.

Keywords: quantum ring, strain distribution, electronic structure
PACC: 0365, 2110, 4620

1. Introduction

Progress in semiconductor growth technology has made it possible to fabricate self-organized quantum ring (QR) materials either by molecular beam epitaxy (MBE) or droplet epitaxy.[1−4] Just like quantum dots (QDs), QRs possess atom-like properties, which make them potentially applicable in electronics, optics and optoelectronic devices.[5,6] Recently, QRs have attracted much more interest for their applications in the fields of quantum information processing and quantum computing.[7,8] It has been demonstrated that both the shape and size of QRs can be controlled by tuning the growth parameters, such as growth temperature, growth rate, annealing progress, and growth interruptions. The shape and geometry parameters are very important for the electronic structure and optical performance of QRs. In early work on QR electronic structure calculations, strain effects are often ignored completely or simplified as constants in the QRs and zero in the surrounding barriers.[9−11] In this paper, we discuss the effects of strain on the electronic structures of QRs. The strain and piezoelectric effects are also taken into account. We use the continuum elastic theory to determine the strain distributions. The effects of strain on the electronic structure are based on the eight-band $\boldsymbol{k}\cdot\boldsymbol{p}$ theory. The piezoelectric effects are taken into consideration up to the second order. The dependence of the electron and heavy-hole wavefunctions due to strain and geometry parameters are then demonstrated.

2. Strain calculations

For convenience, the dependence of the strain components on stress can be set up by using a stiffness matrix $\boldsymbol{D}$, and then the strain and stress may be expressed as two column vectors[12]

$$\boldsymbol{\varepsilon} = \begin{pmatrix} \varepsilon_{xx} \\ \varepsilon_{yy} \\ \varepsilon_{zz} \\ \varepsilon_{xy} \\ \varepsilon_{yz} \\ \varepsilon_{zx} \end{pmatrix} = \begin{pmatrix} \partial u/\partial x \\ \partial v/\partial y \\ \partial w/\partial z \\ (\partial u/\partial y + \partial v/\partial x)/2 \\ (\partial v/\partial z + \partial w/\partial y)/2 \\ (\partial u/\partial z + \partial w/\partial x)/2 \end{pmatrix}, \quad (1a)$$

*Project supported by the National High Technology Research and Development Program of China (Grant No 2009AA03Z405), the National Natural Science Foundation of China (Grant Nos 60908028 and 60971068) and the High School Innovation and Introducing Talent Project of China (Grant No B07005).
†Corresponding author. E-mail: liuyumintech@hotmail.com

and

$$\boldsymbol{\sigma} = \begin{pmatrix} \sigma_{xx} \\ \sigma_{yy} \\ \sigma_{zz} \\ \sigma_{xy} \\ \sigma_{yz} \\ \sigma_{zx} \end{pmatrix} = \boldsymbol{D}(\varepsilon - \varepsilon_0) + \sigma_0, \tag{1b}$$

where u, v, w are the displacements along the coordinates in the x, y and z directions respectively. For a cubic crystal the $\boldsymbol{D}$ matrix can be expressed as

$$\boldsymbol{D} = \begin{pmatrix} C_{11} & C_{12} & C_{12} & 0 & 0 & 0 \\ C_{12} & C_{11} & C_{12} & 0 & 0 & 0 \\ C_{12} & C_{12} & C_{11} & 0 & 0 & 0 \\ 0 & 0 & 0 & C_{14} & 0 & 0 \\ 0 & 0 & 0 & 0 & C_{14} & 0 \\ 0 & 0 & 0 & 0 & 0 & C_{14} \end{pmatrix}. \tag{2}$$

As can be seen, there exist three independent elastic constants. The lattice constants in the QR system are a function of coordinates, therefore the elastic energy of the QR system should be expressed as an integral equation

$$U = \frac{1}{2} \iiint \sigma^{\mathrm{T}} \left(\varepsilon - \varepsilon_0\right) \mathrm{d}v. \tag{3}$$

The components of ε_0 and σ_0 are the initial strain and initial stress in the system; the initial stress in all the regions is taken to be zero, the initial strain is the lattice mismatch of the heterostructure in the QR region and zero in the surrounding barriers. The lattice mismatch is expressed as: $f_0 = (a_d - a_b)/a_b$, for the InAs/GaAs material, $f_0 = -0.067$. So the initial strain in quantum dots is represented as

$$\boldsymbol{\varepsilon}_0 = \begin{pmatrix} f_0 & f_0 & f_0 & 0 & 0 & 0 \end{pmatrix}^{\mathrm{T}}. \tag{4}$$

Substituting Eqs.(4) and (1) into expression (3), the formula of the elastic strain energy turns into

$$\begin{aligned} U = \frac{1}{2} \int [& C_{11}(\varepsilon_{xx}^2 + \varepsilon_{yy}^2 + \varepsilon_{zz}^2) \\ & + C_{12}(\varepsilon_{xx}\varepsilon_{yy} + \varepsilon_{yy}\varepsilon_{zz} + \varepsilon_{zz}\varepsilon_{zxx}) \\ & + 2C_{44}(\varepsilon_{xy}^2 + \varepsilon_{yz}^2 + \varepsilon_{zx}^2) \\ & - 2\varepsilon_0(C_{11}/2 + C_{12})(\varepsilon_{xx} + \varepsilon_{yy} + \varepsilon_{zz}) \\ & + 3\varepsilon_0^2(C_{11}/2 + C_{12})] \mathrm{d}v. \end{aligned} \tag{5}$$

In this paper we use the finite element method to calculate the strain energy.[13−15] The elastic energy is minimized by the conjugate gradient algorithm. When the system elastic energy reaches the minimum value, the lattices are stable after relaxation. In our simulations, the QR is embedded in a rectangular box. The boundary conditions are as follows: the four side faces are fixed along the direction normal to the side faces, and this is a periodic boundary condition, which reflects the strain coupling of the neighbor QR; the bottom side is fixed along the normal direction to simulate the effect of thick substrate in a finite geometry model and the up surface is free for all directions. For more details, see Ref.[16].

3. Piezoelectric effects

Under an applied stress, some semiconducting materials will develop an electric moment whose magnitude is proportional to the stress. The induced linear polarization $\boldsymbol{P}$ can be related to either the strain tensor or the stress tensor. In this work $\boldsymbol{P}$ is expressed by the piezoelectric coefficients e_{ilm} as follows:

$$P_i = \sum_{lm} e_{ilm}(r)\varepsilon_{lm}(r). \tag{6}$$

In the common matrix representation this is written as

$$\begin{pmatrix} P_x \\ P_y \\ P_z \end{pmatrix} = \begin{pmatrix} e_{11} & e_{12} & e_{13} & e_{14} & e_{15} & e_{16} \\ e_{21} & e_{22} & e_{23} & e_{24} & e_{25} & e_{26} \\ e_{31} & e_{32} & e_{33} & e_{34} & e_{35} & e_{36} \end{pmatrix} \begin{pmatrix} \varepsilon_{xx} \\ \varepsilon_{yy} \\ \varepsilon_{zz} \\ 2\varepsilon_{yz} \\ 2\varepsilon_{zx} \\ 2\varepsilon_{xy} \end{pmatrix}. \tag{7}$$

For InAs/GaAs crystals with zinc-blended structure, all components of e_{ij} are zero except $e_{14} = e_{25} = e_{36}$, leading to the simple relationship

$$\begin{pmatrix} P_x \\ P_y \\ P_z \end{pmatrix} = \begin{pmatrix} e_{14} & 0 & 0 \\ 0 & e_{14} & 0 \\ 0 & 0 & e_{14} \end{pmatrix} \begin{pmatrix} 2\varepsilon_{yz} \\ 2\varepsilon_{zx} \\ 2\varepsilon_{xy} \end{pmatrix}. \tag{8}$$

Recently, Bester *et al* proposed that the second order polarization is as important as the linear polarization for InAs/GaAs heterostructure materials,[17] and they derived the second order piezoelectric tensors by using density functional theory. The second order polarization is expressed as

$$Q_\lambda = \frac{1}{2} \sum_{i,j,k,l} \tilde{B}_{\lambda,ij,kl}\varepsilon_{i,j}\varepsilon_{k,l}, \tag{9}$$

where $\lambda,\ i,\ j,\ k,\ l \in x,\ y,\ z$ and $\tilde{\boldsymbol{B}}$ is the polarization tensor. For InAs/GaAs there are only three

parameters and the second order polarization can be simplified as

$$\boldsymbol{Q} = 2B_{114}\begin{pmatrix}\varepsilon_{xx}\varepsilon_{yz}\\ \varepsilon_{yy}\varepsilon_{xz}\\ \varepsilon_{zz}\varepsilon_{xy}\end{pmatrix} + 2B_{124}\begin{pmatrix}\varepsilon_{yz}\left(\varepsilon_{yy}+\varepsilon_{zz}\right)\\ \varepsilon_{xz}\left(\varepsilon_{xx}+\varepsilon_{zz}\right)\\ \varepsilon_{xy}\left(\varepsilon_{xx}+\varepsilon_{yy}\right)\end{pmatrix} + 4B_{156}\begin{pmatrix}\varepsilon_{xz}\varepsilon_{xy}\\ \varepsilon_{yz}\varepsilon_{xy}\\ \varepsilon_{yz}\varepsilon_{xz}\end{pmatrix}. \quad (10)$$

The values of B_{114}, B_{124} and B_{156} used for the calculation are –0.439, –3.765, –0.492 for GaAs and –0.531, –4.076, –0.120 for InAs, respectively, and the unit is C/m^2. The fixed piezoelectric charge density is obtained from the divergence of the total polarization

$$\rho\left(r\right) = -\nabla\cdot\left(\boldsymbol{P}+\boldsymbol{Q}\right). \quad (11)$$

The piezoelectric potential V_{P} is obtained from the Poisson equation

$$\varepsilon_0\nabla\cdot\left(\varepsilon_{\mathrm{r}}(r)\nabla V_{\mathrm{P}}\right) = \rho, \quad (12)$$

where ε_0 and ε_{r} are the dielectric constant in vacuum and the relative static dielectric tensor respectively.

4. Electronic structure calculations

The electronic structure is calculated in the single-band envelope approximation with the modified band edge from the eight-band $\boldsymbol{k}\cdot\boldsymbol{p}$ theory. The electron and heavy-hole Hamiltonians are[18–20]

$$H_{\mathrm{e}} = -\frac{\hbar^2}{2m^*}\nabla^2 + E_{\mathrm{c}} + a_{\mathrm{c}}\varepsilon_{\mathrm{hyd}} - eV_{\mathrm{P}}, \quad (13a)$$

and

$$H_{\mathrm{hh}} = -\frac{\hbar^2}{2m^*_{\mathrm{hh}}}\nabla^2 + E_{\mathrm{v}} + a_{\mathrm{v}}\varepsilon_{\mathrm{hyd}} + b\varepsilon_{\mathrm{bi}} - eV_{\mathrm{P}}, \quad (13b)$$

where E_{c} and E_{v} are the local conduction-band and heavy-hole-band edges in the absence of strain, a_{c} and a_{v} are the conduction-band and valence-band deformation potentials, $\varepsilon_{\mathrm{hyd}} = \sum_i \varepsilon_{ii}$ is the hydrostatic strain, $\varepsilon_{\mathrm{bi}} = 2\varepsilon_{zz} - (\varepsilon_{xx}+\varepsilon_{yy})$ is the bi-axial strain, m^* and m^*_{hh} are the effective masses of the electron and heavy hole, and e is the charge of one electron. As can be seen from expression (13), the electron and heavy hole Hamiltonians include the effects of the strain modified conduction band edge and the piezoelectric potential energy. The values of all kinds of material parameters used for calculations are given in Table 1.[21]

Table 1. The material parameters of InAs/GaAs used for calculations.

	m^*	ε_{r}	C_{11}	C_{12}	C_{44}	E_{c}	a_{c}	E_{v}	e_{14}	a_{v}	b
InAs	0.04	15.2	83.4	45.4	39.5	0.67	–5.08	0.25	0.045	1	–1.8
GaAs	0.0667	12.9	118.8	53.8	59.4	1.519	–7.17	0	0.16	1.16	–1.7

5. Results and discussions

We consider a circular InAs QR on GaAs, as has been observed in experiments grown by molecular-beam epitaxy. The wetting layer is ignored completely just as in most studies of QDs. The height of the quantum dot is 5 nm, the inner and outer radii of the QR are 10 nm and 20 nm, respectively. The cross section of the QR is an ellipse with long and short semi-axes of 5 and 2.5 nm respectively. The simulation box of the GaAs is 80 nm along the transverse direction and 50 nm along the growth direction. The QR is located at the centre of the GaAs box. The growth direction is along the [001] direction. The geometry model is shown in Fig.1.

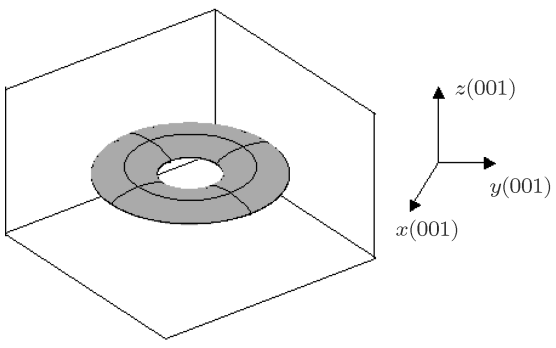
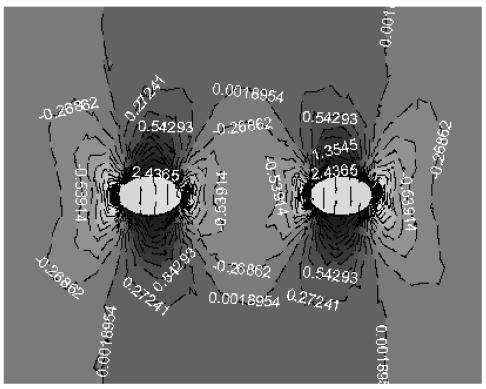
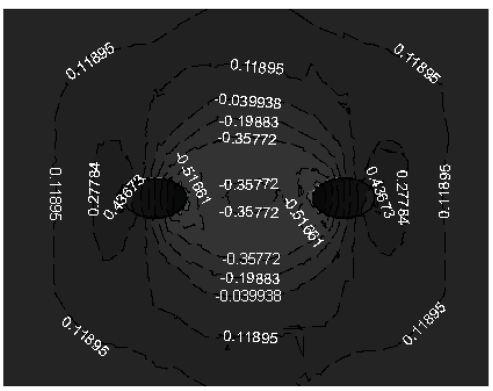


Fig.1. Schematic drawing of the geometry of QR.

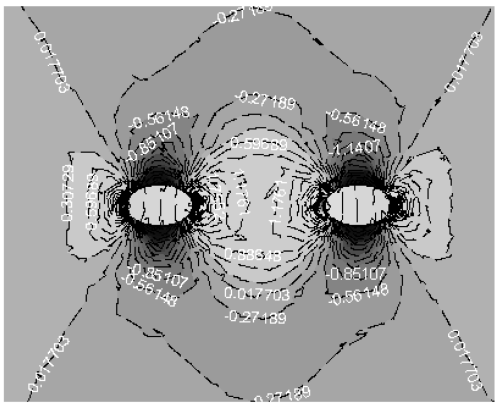
The strain distributions are visualized in Fig.2, where ε_{xx}, ε_{yy}, ε_{zz} and ε_{xz} strain distributions correspond to Figs.2(a), 2(b), 2(c) and 2(d), respectively. Figures 2(e) and 2(f) are the hydrostatic strain and bi-axial strain, which are very important for the deformation potential of the conduction band and valence band edges. The strain distributions shown in Figs.2(a)–2(f) are the cross sections of the (010) plane through the centre of the QR. From Fig.2, one can notice that the normal strain (ε_{xx}, ε_{yy} and ε_{zz}) distributions are symmetric about the z-axis; however, the shear strain (Fig.2(d)) is not symmetric about the z-axis. As shown in Figs.2(a) and 2(b), the tensile strains are mainly distributed around the QR. The compressive strain in the QR is relaxed from the initial value –0.067 to about –0.05. The ε_{zz} strain distribution, due to the Poisson effect, shows a compressive strain around the QR and a tensile strain in the QR. From Fig.2(d), the shear strain is mainly focused on the boundary region between the QR and the surrounding barriers, and outside the boundary region the shear strain is quickly decreased to zero. In all the contour plot figures, we do not show the strain distributions in the QR, the details of which can be found in Figs.2(f) and 2(h). From Figs.2(e)–2(h), it can be seen that in the inner part of the QR, the hydrostatic strain value is almost constant, while the hydrostatic strain value in the barrier region is very small and near zero. In the regions above the QR, one can see a compressive strain induced by the buried QR, which suggests that, during the growth of a subsequent sheet of QR, there is a tendency for the QR to be formed at the region with compressive strain, implying a reduction of energy in forming a cluster of atoms or a new QR. The details of the strain distributions for the normal strain, hydrostatic strain and bi-axial strain can be found in Figs.2(f) and 2(h), where the strain distributions scanning through the x-axis and the centre of the QR are shown. It is very clear that all the strain components are symmetrically distributed about the x-axis, and this is because the simulated QR is an ideal circle and symmetric about the z-axis.



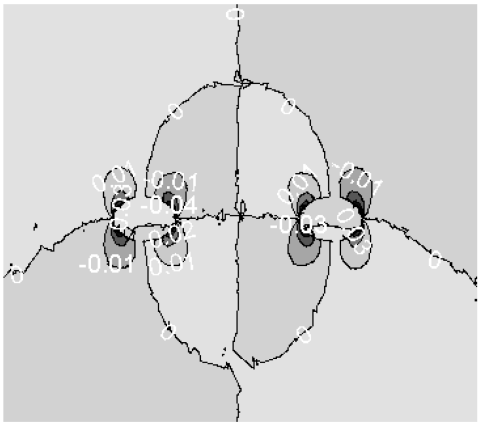
(a)



(b)



(c)



(d)

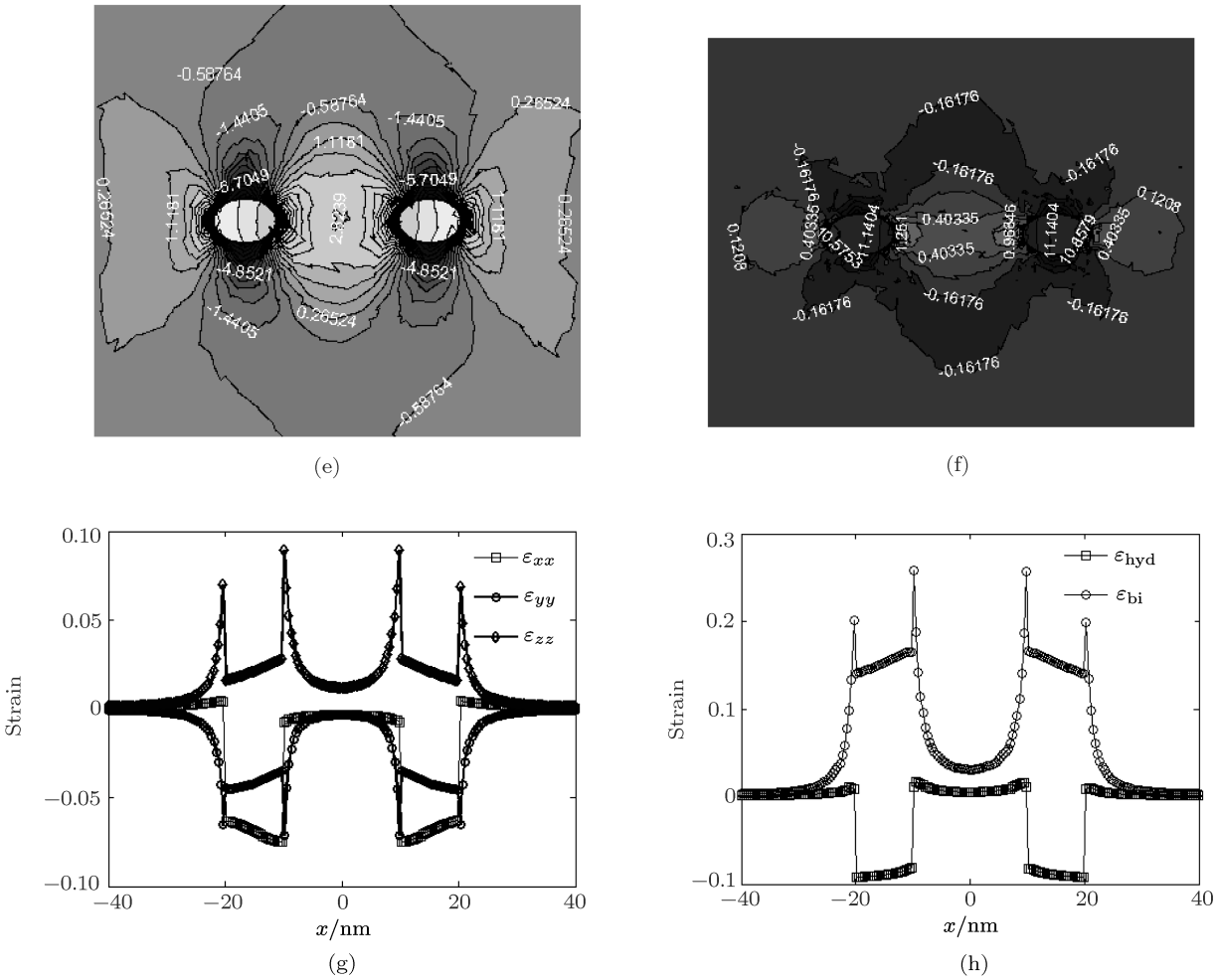


Fig.2. The strain distribution in the (010) plan through the centre of the QR. (a), (b), (c) and (d) are the ε_{xx}, ε_{yy}, ε_{zz} and ε_{xz} strain components, respectively. (e) and (f) show the hydrostatic $\varepsilon_{\rm hyd}$ and bi-axial $\varepsilon_{\rm bi}$ strain. (g) and (h) show the normal strain, hydrostatic and bi-axial strain distribution along the x-axis.

From Eq.(8), the strength of the linear polarizations is only dependent on the shear strain components; however, the polarizations of the second order are influenced by both the normal and the shear strain as can be seen in Eq.(10). The strain analysis in Fig.2(e) has shown that the shear strain is mainly focused near the interface of QR and its surrounding barriers. Figure 3(a) shows the 3D piezoelectric potential distribution. It is very clear that the piezoelectric potential mainly distributes near the regions of the boundary of the QR, which is just like the distributions of shear strain components. The piezoelectric potential distributions show that the shear strain produces domain contributions to both linear and nonlinear polarization. To show more detailed information about the piezoelectric potential, we show the piezoelectric potential distribution on the (001) surface with $z = 10$ nm in Fig.3(b). In Figs.3(c) and 3(d), we show the piezoelectric potential distribution on the (100) surface with $x = 8$ nm and $x = 22$ nm, respectively. For the surface of $x = 8$ nm, we can see that the piezoelectric potential is mainly distributed near the regions of inner boundary of the QR. For the surface of $x = 15$ nm, we can see that the piezoelectric potential is mainly distributed near the regions of the outer boundary of the QR. However, it should be noted that the piezoelectric potential is mainly distributed in the barrier regions, since the linear piezoelectric coefficient e_{14} of GaAs is about four times larger than that of InAs, further, the second order piezoelectric coefficients of GaAs are also bigger than those of InAs. It is clear from Fig.3(a) that the inclusion of $V_{\rm P}$ in the confinement potential will change the symmetry of the QR about the z-axis from C_∞ to $C_{2\rm v}$. In Fig.3(e),

the strain modified band edges for conduction-band, heavy-hole-band, light-hole-band and spin-splitting-band along the x-axis are shown. In plotting Fig.3(e), we select the unstrained GaAs valence band edge as the energy of zero, so the unstrained conduction band edges of InAs and GaAs are 0.67 and 1.519 eV, respectively. The unstrained valence band is degenerate (heavy-hole and light-hole) and for InAs is 0.25eV. The unstrained spin splitting band edges of InAs and GaAs are –0.38 eV and –0.34 eV, respectively. As can be seen, the dominant effects of the strain are that the QR exhibits a large increase in its band gap due to the considerable hydrostatic strain. For example, the conduction band in the QR raises its band edge from 0.67 eV to about 1.1 eV, which greatly reduces the electron confinement in the well. The valence band has a more complicated structure due to breaking the degeneracy and forming the heavy-hole and light-hole.[10]

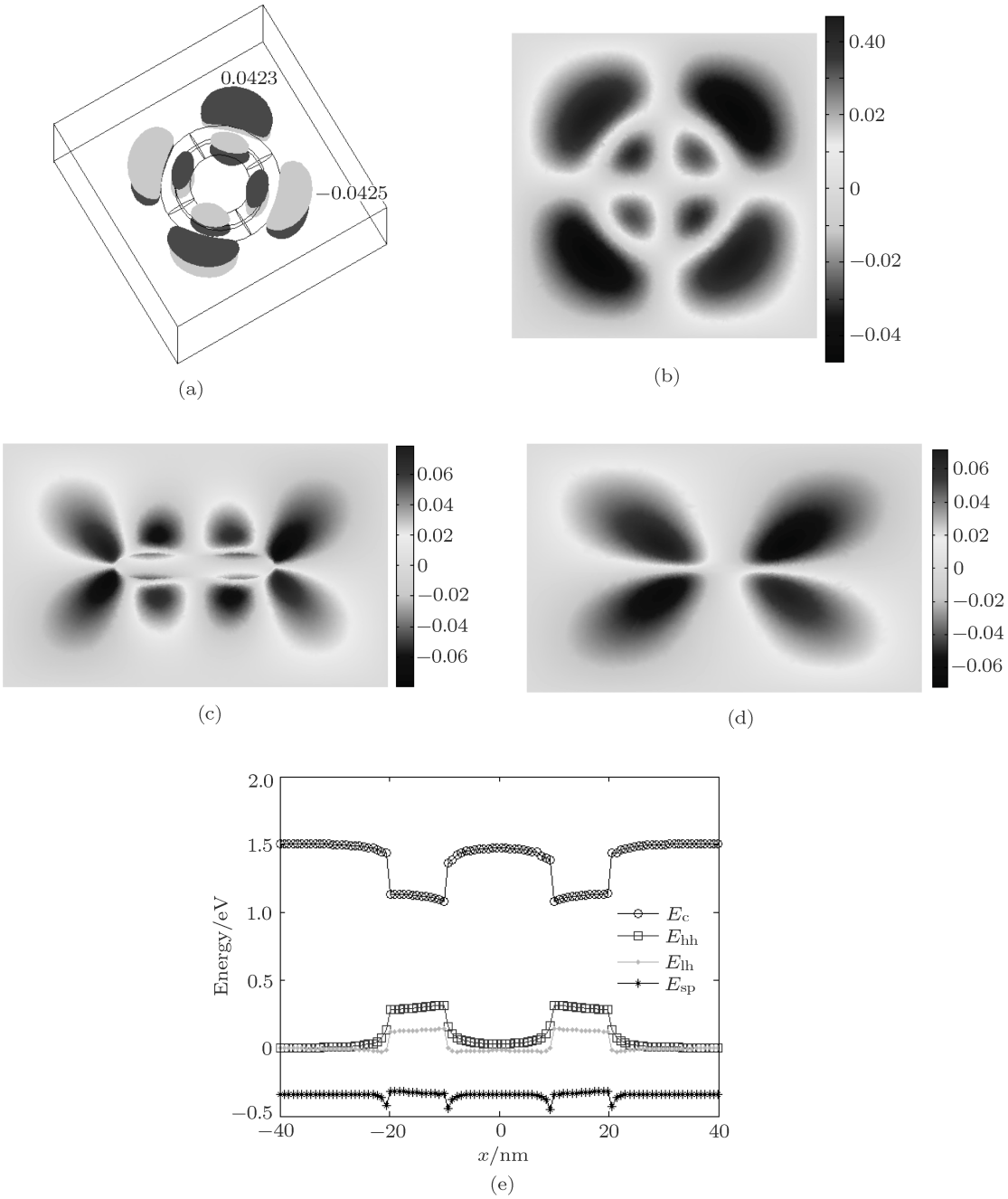
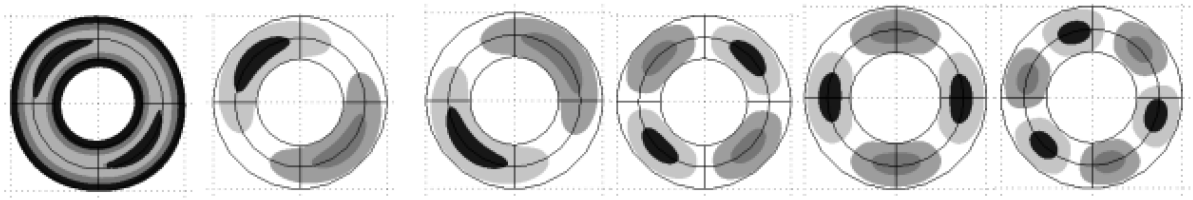


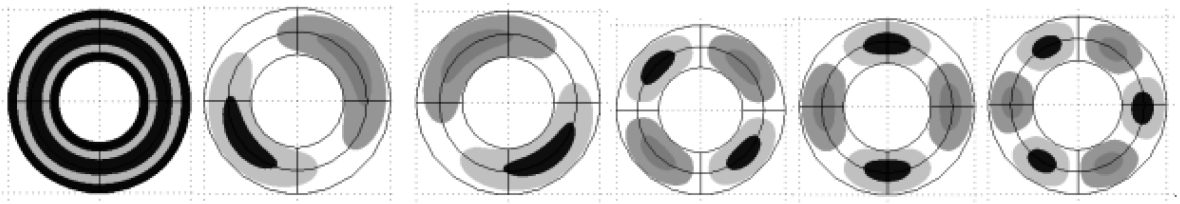
Fig.3. (a) The 3D isosurface for the piezoelectric potential. (b) The piezoelectric potential distribution on the (001) surface with $z = 10$ nm. (c) and (d) are the piezoelectric potential distribution on the (100) surface with $x = 8$ nm and $x = 22$ nm respectively. (e) The band edge distribution along the (001) direction with $z = y = 0$ nm.

We now consider the electronic energy levels of the ideal QR. The bound states are determined by numerically solving the Hamiltonian expression (13). The calculated electron energy levels for the ground state and the first few excited states in the conduction band are shown in Figs.4(a) and 4(b). For the bound state wavefunction distribution, those with and without considering the piezoelectric effect are shown in Figs.4(a) and 4(b). We can see that the piezoelectric potential has no obvious influence on the energy levels of the electron. The difference of the energy level for the corresponding bound state is only about 0.4 meV. However, the influence of the piezoelectric potential on the wavefunction distributions is very obvious. The heavy-hole energy levels and wavefunction distributions are shown in Fig.5. It is easy to see that the presence of the piezoelectric potential leads to an obvious influence on both the energy levels and wavefunction distributions. The difference of the energy level for the corresponding bound state is about 0.002 eV. The wavefunction distributions of the electron and heavy-hole are very sensitive to the anisotropic characteristics of the absorption spectrum.



$E = 1.300626$ eV $E = 1.303146$ eV $E = 1.304327$ eV $E = 1.312139$ eV $E = 1.313577$ eV $E = 1.327534$ eV

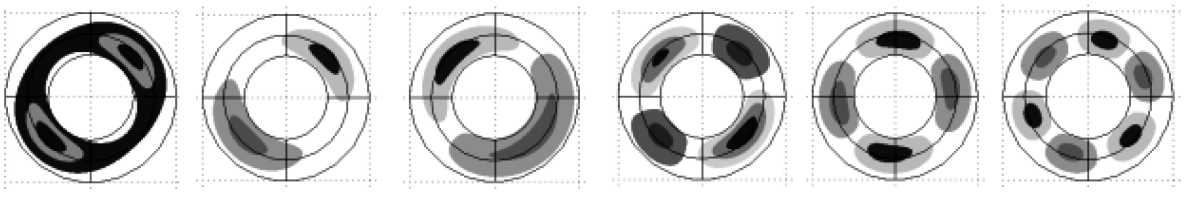
(a)



$E = 1.301072$ eV $E = 1.304145$ eV $E = 1.304146$ eV $E = 1.312678$ eV $E = 1.313781$ eV $E = 1.327964$ eV

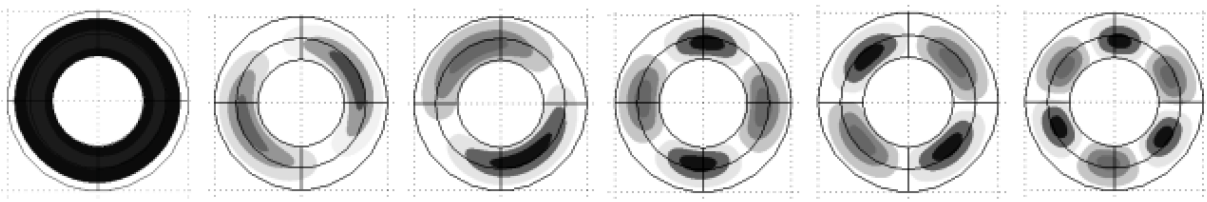
(b)

Fig.4. A contour plot view of the first few electron wavefunction distributions with piezoelectric potential effect (a) and without piezoelectric potential (b).



$E = -0.263142$ eV $E = -0.263602$ eV $E = -0.261426$ eV $E = -0.260702$ eV $E = -0.260071$ eV $E = -0.258186$ eV

(a)



$E = -0.261181$ eV $E = -0.260687$ eV $E = -0.260667$ eV $E = -0.259218$ eV $E = -0.259145$ eV $E = -0.256712$ eV

(b)

Fig.5. A contour plot view of the first few heavy-hole wavefunction distributions with piezoelectric potential effect (a) and without piezoelectric potential (b).

In Fig.6, the electron and heavy-hole energy levels as functions of the vertical radius of the QR are shown. In calculating the energy level, the transverse inner radius and outer radius are fixed to be 10 nm and 20 nm, respectively. It can be seen that the energy level of the electron will decrease on increasing the height of the QR from 2 nm to 10 nm. For the heavy-hole, the energy level will firstly increase and then decrease on increasing the height of the QR, and the critical point is reached when the height is about 4 nm (the corresponding vertical radius is 2 nm).

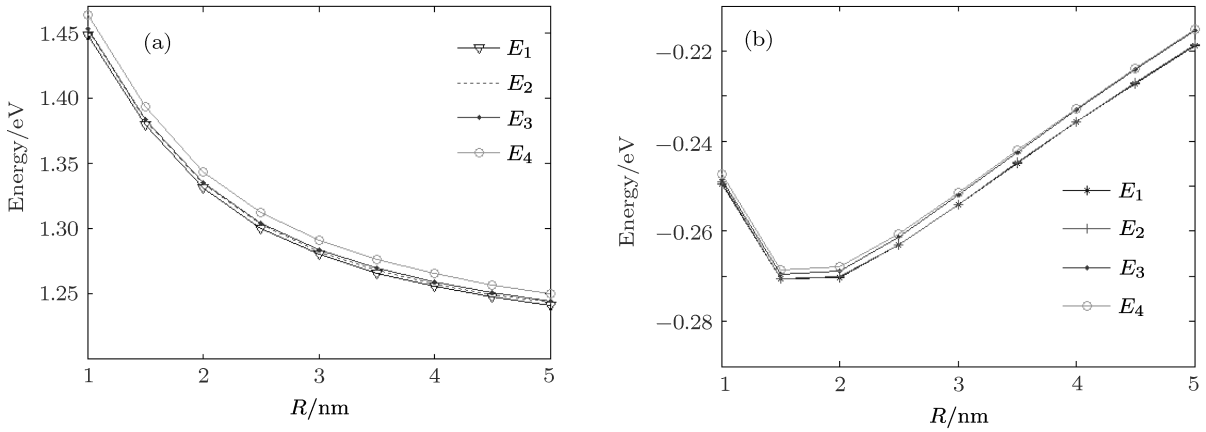


Fig.6. The electron (a) and heavy-hole (b) energy levels as functions of the vertical radius of the QR, with inner and outer radii of 10 nm and 20 nm, respectively.

So far, we have discussed the dependence of the electron and hole's energy levels on strain, piezoelectric effects and geometrical parameters of QR in 3D. However, there are some limitations to our simulation model. First, in calculating the electronic structure, the more accurate valence band intermixing effects are not included. To take such effects into consideration, a complex multi-band effective mass theory should be used.[22] Second, the interaction of carriers is ignored. If only the Coulomb effect is taken into consideration, it is easy to integrate this effect with our model by iteration calculations.[23] Third, the spin–orbit interaction (SOI), which is an interesting field because of its potential application in all electrically controlled spintronic devices,[24,25] is completely ignored in our model. All these limitations of our model should be considered in future investigations.

6. Conclusions

The relaxation of the strain and its residual components in the self-organized InAs/GaAs QR are calculated using the continuum elastic theory. As an example, we investigated an ideal circular QR without considering the effects of the wetting layer. By taking into account the influences of the strain and the piezoelectric potential on the band edge, we have solved the three-dimensional, effective mass single-band Schrödinger equation for both the electron and heavy-hole. The energy levels and the corresponding wavefunctions are calculated. The calculated results show that the influence of both strain and piezoelectric effects are very important for the electronic structure and optical characteristics of the InAs/GaAs QR. The calculated results agree with the published literature.

References

[1] Huang S H, Niu Z C, Fang Z D, Ni H Q, Gong Z and Xia J B 2006 *Appl. Phys. Lett.* **89** 031921

[2] Cui J, He Q, Jiang X M, Fan Y L, Yang X J, Xue F and Jiang Z M 2003 *Appl. Phys. Lett.* **83** 2907

[3] Liu Y M, Yu Z Y and Ren X M 2009 *Chin. Phys.* B **18** 0009

[4] Lin J H, Yang H B, Qin J, Zhang B, Fan Y L, Yang X J and Jiang Z M 2007 *J. Appl. Phys.* **101** 083528

[5] Zhou Z Q, Xu Y Q, Hao R T, Tang B, Ren Z W and Niu Z C 2008 *J. Appl. Phys.* **103** 094318

[6] Lin Y M, Yu Z Y, Yang H B, Zhang N, Feng Q and Zhang X G 2005 *Opt. Commun.* **246** 367
[7] Luis G G V, Dias Da Silva, Jose M V B and Sergio E U 2007 *Phys. Rev.* B **76** 155306
[8] Dong Q R, Li S S, Niu Z C, Feng S L and Zheng H Z 2004 *J. Appl. Phys.* **96** 3277
[9] Filikhin I, Deyneka E and Vlahovic B 2004 *Model Simulat. Mater. Sci. Eng.* **12** 1121
[10] Li S S and Xia J B 2002 *J. Appl. Phys.* **91** 3227
[11] Wang G X and Zhang P 2008 *J. Appl. Phys.* **103** 063713
[12] Liu Y M, Yu Z Y and Ren X M 2008 *Chin. Phys.* B **17** 3471
[13] Liu Y M, Yu Z Y and Huang Y Z 2006 *Int. J. Modern Phys.* B **20** 4899
[14] Liu Y M, Yu Z Y, Yang H B and Huang Y Z 2006 *Acta Phys. Sin.* **55** 5023 (in Chinese)
[15] Liu Y M, Yu Z Y and Huang Y Z 2007 *J. University Sci. Technol. Beijing* **14** 477
[16] Benabbas T, Androussi Y and Lefebvre A 1999 *J. Appl. Phys.* **86** 1945
[17] Bester G, Zunger A, Wu X F and Vanderbilt D 2006 *Phys. Rev.* B **76** 081305
[18] Sidor Y, Partoens B, Peeters F M, Ben T, Ponce A, Sales D L and Gonzalez Y 2007 *Phys. Rev.* B **75** 125120
[19] Liu Y M, Yu Z Y and Ren X M 2008 *Chin. Phys. Lett.* **25** 1850
[20] Liu Y M, Yu Z Y and Ren X M 2009 *Chin. Phys.* B **18** 0016
[21] Liu Y M, Yu Z Y and Ren X M 2009 *Chin. Phys.* B **18** 0881
[22] Chang K, Li S S, Xia J B and Peeters F M 2004 *Phys. Rev.* B **69** 235203
[23] Chang K, Xia J B and Peeters F M 2003 *Appl. Phys. Lett.* **82** 2661
[24] Sheng J S and Chang K 2006 *Phys. Rev.* B **74** 235315
[25] Wang M and Chang K 2008 *Phys. Rev.* B **77** 125330